Optimizing a CATR Quiet Zone using an Array Feed

C.G. Parini, R. Dubrovka
Queen Mary University of London
School of Electronic Engineering and Computer Sciences
Peter Landin Building,
London UK E1 4FZ
c.g.parini@qmul.ac.uk, r.dubrovka@qmul.ac.uk

S.F. Gregson
NSI-MI Technologies LLC.
19730 Magellan Drive,
Torrance, CA 90502 USA
sgregson@nsi-mi.com

Abstract*—The efficiency of use of the parabolic reflector of a single offset reflector compact antenna test range (CATR) is affected largely by the illumination provided by the range feed and the reflector edge treatment. Thus, when these factors are taken together it is commonly found that the realized quiet zone (QZ) diameter is typically as little as 30% of the diameter of the reflector for the commonly encountered case of a single offset CATR. Furthermore, single offset CATR performance is known to degrade as the wavelength of the illuminating fields becomes more comparable with the physical dimensions of the reflector because the physical optics (PO) assumption needed for collimation of the reflected field becomes less effective. Different reflector edge treatments such as rolled or serrated edges are commonly employed to taper the intensity of the reflected fields at the reflector aperture boundary, seeking to minimize the level of diffracted fields in the quiet-zone (QZ). Such strategies mean that at higher frequencies the transverse dimensions of the QZ are unnecessarily reduced thereby decreasing the spatial efficiency of the CATR and limiting the effective bandwidth of the antenna test system. In this paper we report preliminary results that begin to investigate the alternative strategy for controlling the signal illuminating the CATR reflector by utilising a shaped beam feed antenna. Building on our previously reported work of efficient CATR computational electromagnetic simulation, we report the use of an array feed whose excitation is optimized to achieve maximum QZ size. We illustrate the concept by employing the technique with a sector-shaped, reflector single offset CATR having no edge treatment and then using the same reflector with an edge treatment and by examining the impact that this has on the amplitude taper and the amplitude and phase peak-to-peak ripple.

I. INTRODUCTION

The single-offset compact antenna test range (CATR) is a widely deployed technique for broadband characterization of electrically large antennas at reduced range lengths [1]. The nature of the curvature and position of the offset parabolic reflector as well as the edge geometry ensures that the resulting collimated field is comprised of a pseudo transverse electric and magnetic (TEM) wave. Thus, by projecting an image of the feed at infinity, the CATR synthesizes the type of wave-front that would be incident on the antenna under test (AUT) if it were located very much further away from the feed than is actually the case with the coupling of the plane-wave into the aperture of the AUT creating the classical measured "far-field" radiation pattern. The accuracy of a pattern measured using a CATR is primarily determined by the phase and amplitude quality of the pseudo plane-wave incident on the AUT aperture, with this being restricted by two main factors: amplitude taper (which is imposed by the pattern of the feed), and reflector edge diffraction, which usually manifests as a high spatial frequency ripple in the pseudo plane wave [2]. It has therefore become customary to specify CATR performance in terms of amplitude taper, and amplitude & phase ripple of this wave over a volume of space, termed the quiet zone (QZ). Unfortunately, in most cases it is not directly apparent how a given QZ performance specification will manifest itself on the resulting antenna pattern measurement. However, with the advent of powerful digital computers and highly-accurate computational electromagnetic (CEM) models, it has now become possible to extend the CATR electromagnetic simulation to encompass the complete CATR AUT pattern measurement process thereby permitting quantifiable accuracies to be easily determined prior to actual measurement. An extensive study of the accuracy of this approach was reported by the writers at the AMTA 2015 symposium [3].

Amplitude and phase ripple of the quiet zone is still the dominant performance criteria of a given CATR facility with an industry standard being ±0.5dB and ±5° amplitude and phase ripple respectively defining the QZ dimension [1]. These performance criteria are usually determined experimentally by probing the QZ with a planar scanner using either plane-polar or plane-rectilinear scanning. In a recent paper [4] the authors have detailed the CEM simulation of the measurement of a CATR QZ using arbitrary but known near-field probes using both the Plane Wave Spectrum (PWS) and Reaction Integral (RI) based modelling techniques. These models include effects associated with cross polarisation and polarisation purity of the respective scanning field probes and so it is possible to utilise measured *or* simulated patterns for the field probe to predict the "measured" QZ performance.

This paper extends the above work by presenting the results of a preliminary design study using an array of waveguide elements as the feed to optimally control the illumination of the CATR reflector. CATR performance is known to degrade as the wavelength of the illuminating fields becomes more comparable with the physical dimensions of the reflector when the physical optics (PO) needed for collimation of the reflected field becomes less effective [1, 5]. The curvature and position of the parabolic reflector as well as its edge treatment ensures that the resulting collimated field comprises a pseudo transverse electric and magnetic (TEM) wave with minimal diffraction related effects. A number of different edge treatments can be employed to taper the intensity of the

reflected fields at the reflector aperture boundary with two of the most commonly encountered techniques requiring the edges of the reflector to be either rolled or serrated [1]. Such treatments seek to minimize the level of diffracted fields in the quiet-zone (QZ) however these strategies mean that at higher frequencies the transverse dimensions of the QZ are unnecessarily reduced thereby decreasing the spatial efficiency of the CATR and limiting the effective bandwidth of the antenna test system [1]. An alternative strategy for tapering the reflected field at the edge of the CATR aperture is to illuminate the edge with a shaped beam such that the edges coincide with "ideally" a pattern null [6]. Typically, electrically small radiators such as circular choked horns are used to feed CATR reflectors as these maximize the uniformity of illumination across much of the reflector surface which serves to minimize the amplitude taper in the QZ, but leads to high edge illumination and hence the need for edge "treatment" [1]. However the use of a feed array enables a far greater degree of control over the feeding pattern which can then be harnessed to maximize uniformity of illumination over some portion of the reflector whilst also providing the field intensity windowing needed to minimize edge diffraction effects thereby enabling greater aperture efficiency to be achieved for a given reflector size [1]. Thus, for a fixed QZ dimension a smaller CATR can be utilized thereby providing significant savings in the manufacturing cost of the reflector and anechoic chamber. In the following sections we present a new efficient CATR computational electromagnetic simulation that enables a feed array to be included within the design optimization loop. This new highly efficient technique also includes mutual coupling effects [7, 8] which tend to govern the cross-polar performance of the overall CATR system and allows matching to non-circular, *e.g.* sector-shaped, reflectors [9].

II. Overview of the CATR Configuration and its Simulation

To illustrate the concept we use the sector-shaped single offset reflector CATR having no edge treatment presented in Figure 1 [9]. This 3m 18 panel CATR forms the 8GHz to 60GHz CATR facility at Queen Mary University of London's (QMUL) Antenna Measurement Laboratory.

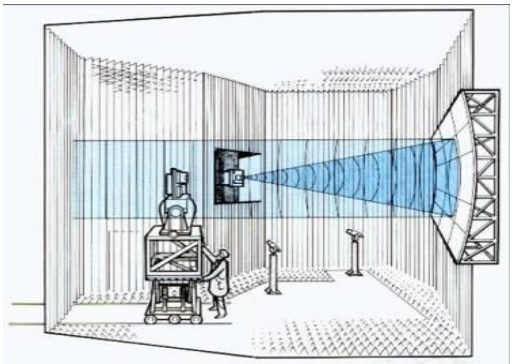

Figure 1. Schematic representation of sector-shaped single offset reflector CATR at Queen Mary University of London

The offset parabolic reflector has a 5.4m focal length and an overall surface accuracy of approximately 80microns. In our computational electromagnetic (CEM) model the surface profile of the CATR is assumed to be formed from a perfect concave paraboloidal surface, and the reflector has no edge treatment being modelled as a perfect metallic knife-edge. Imperfections can be included within the analysis however for the present study these are thought to constitute second order effects and so were omitted. The phase centre of the range's corrugated horn feed is placed at the focus of the offset reflector and the feed is tilted to an angle of 28°, with the edges of the reflector being seen at ±14° about this pointing. At 8GHz the corrugated feed, as shown in Figure 2, has an aperture size of 3.39λ and presents an edge illumination in the azimuth plane of -5.0dB. The simulated field illuminating the reflector is shown in Figure 3.

Figure 2. CATR corrugated horn used for 8.0 to 12.0 GHz operation.

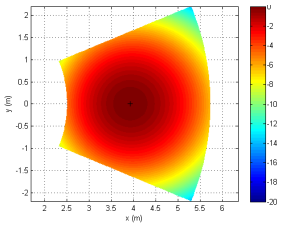

Figure 3. Simulated field of CATR of Figure 1 using a corrugated feed horn operating at 8GHz.

Figure 4 shows the predicted QZ amplitude in both the *x* and *y* dimensions, which exhibit a field taper across the nominal 1m central QZ in the *y*-axis = 0.43dB and in the *x*-axis = 0 .69dB. Here, the amplitude taper is determined from the difference between the maximum and minimum values of the least-squares best fit 2nd order polynomial function along each cut. About this field taper is the QZ amplitude ripple which for the *y*-axis = 0.81dB; and for the *x*-axis = 1.39dB and a phase ripple of y-axis = 5.8°, x-axis = 10.3°. In the next section we replace the corrugated feed horn with an array fed.

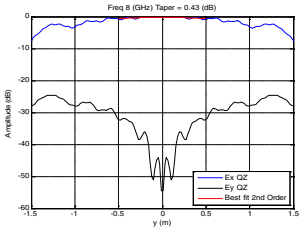

Figure 4a. Principal plane cut of CATR QZ amplitude using the corrugated feed of fig. *y*-axis cut. Field taper in *y*-axis = 0.43dB.

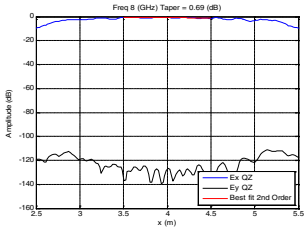

Figure 4b. Principal plane cut of CATR QZ amplitude using the corrugated feed of fig. 2 *x*-axis cut. Field taper in *x*-axis = 0.69dB.

III. CATR Array Feed

A square aperture pyramidal horn is used as the array element and a 3 x 3 element array was employed in the initial study. This can be seen presented in Figure 5c. The aperture dimension of the array element is 0.933λ square, giving a dimension of the overall 9 element array of 2.96λ. As shown in Figure 5a this offers a very similar radiating aperture area to the corrugated horn as used in the previous section. Figure 5b shows the 9 element array with a "clean-beam" amplitude excitation and constant phase of 0°. In order that we can optimise the array excitation to achieve the best QZ for the CATR we require a very fast CEM model for the array to be included in the CEM model of the complete CATR. The elementary theory of arrays separates the array factor and element factor, *i.e.* pattern, in the expression for the array

radiation pattern. However, mutual coupling between the elements causes the element factor to change and become dependent on the element spacing and its precise location within the array. The analysis of mutual coupling in a finite planar array of rectangular apertures embedded in an infinite ground plane was developed by one of us nearly three-decades ago [10]. In practice, the infinite ground plane approximation is not restrictive if the ground plane extends to half a wavelength past the outer active elements. This is because the pattern of a single element surrounded by a half wavelength flange is practically the same as that of a single element embedded within an infinite ground plane [11].

The mutual coupling analysis essentially gives a scattering matrix for the mode coupling between apertures in the half space in front of the array. This is then cascaded with the scattering matrices for the array elements and the associated beamforming network. It is not possible to restrict the mutual coupling analysis just to that between the TE_{10} fundamental modes, as a considerable amount of the total coupled power lies in the higher order modes. Because the method of analysis can be viewed as one of matching the radiated coupled field at an aperture to a finite number of modes, the use of insufficient modes results in the calculation of incorrect mode coupling coefficients. For a given problem, it is difficult to determine in advance the minimum number of modes that should be included within the calculations. Considerable savings in computer time can be made by choosing only the most important modes. For the work presented here we have used the following 12 rectangular waveguide modes: TE_{10}, TE_{01}, TM_{11}, TE_{11}, TE_{20}, TE_{02}, TM_{12}, TE_{12}, TE_{21}, TE_{30}, TE_{03}. The above technique provides a complex but highly accurate analysis for the complete array antenna and is described in detail in the open literature [11].

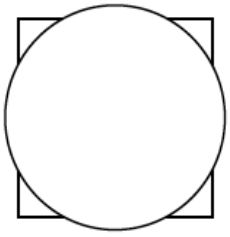

Figure 5a. Comparison of circular corrugated horn aperture, red line, with 3 x 3 element rectangular array aperture, black line.

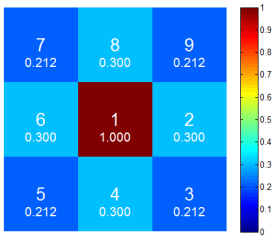

Figure 5b. 9-element array showing element number (top) and excitation amplitude for clean beam (bottom). Uniform phase excitation used.

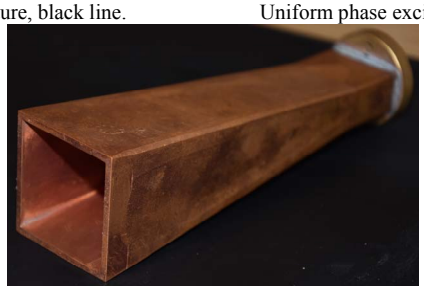

Figure 5c. Flared x-band waveguide horn used as array feed element.

In the array analysis it is important to consider what lies behind the coupled rectangular apertures. In most cases this will be a pyramidal horn tapering into a square or rectangular waveguide. The tapered section of the horn means that propagating higher order modes coupled at the horn aperture will travel down the tapered horn until the cross-section of the horn is such that the higher order mode is cut-off. At this point the mode will be reflected back towards the horn aperture with a reflection coefficient magnitude of near unity. These reflected modes not only alter the aperture field directly, they also cause further mutual coupling, which must be included in an accurate representation. The mutual coupling resulting from this higher order mode itself modifies the aperture field and so on. Fortunately, it is found that this later effect converges very rapidly after as few as 3 iterations [10]. These modes have an associated phase factor resulting from the round trip path-length down the horn to the reflection point plus the phase change occurring at the cut-off point of which is $+\pi/2$ for transverse electric (TE) and $-\pi/2$ for transverse magnetic (TM) modes. For each higher order mode the location of this cut-off point must be determined accurately if the phase of the reflected modes at the horn aperture is to be correctly determined. What is required however is the S-parameters of the horn for each higher order mode used. This can be determined using the technique of modal matching, where the horn is split up into a large number of short waveguide sections, a technique that has been successfully demonstrated by a number of authors [12]. Using this technique, we have developed CEM software to analyse a horn of rectangular cross-section containing steps which can be partially, but symmetrically, filled with dielectric. Horns with smooth flairs can be accurately modelled using a large number of small steps, *i.e.* a staircase approximation. For the array element considered here (*cf.* Figure 5c) the horn flair is 3.15λ long and the flair angle is 6° in the E-plane and 2.9° in the H-plane.

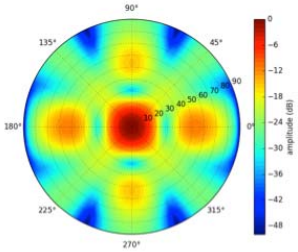

Figure 6a. Copolar radiation patterns of 9 element array including the effects of mutual coupling.

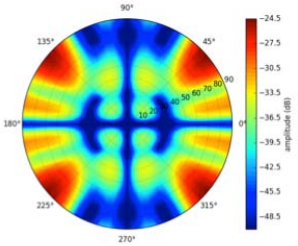

Figure 6b. Cross-polar radiation patterns of 9 element array including the effects of mutual coupling.

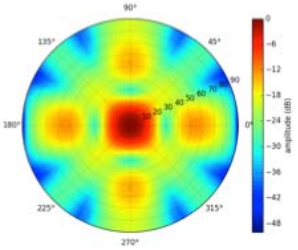

Figure 6c. As per Figure 6a but without the effects of mutual coupling included.

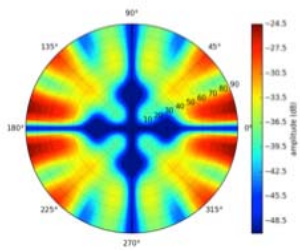

Figure 6d. As per Figure 6b but without the effects of mutual coupling, note the reduction in complexity of the cross-polar pattern.

Since in our analysis we have assumed the horns making up the array to be identical, the S-parameters for each mode only need to be calculated once at the beginning of the program, resulting in no run-time penalty when using this far more accurate representation for the horn. Figure 6a and 6b shows

the computed co-polar and cross-polar far-field amplitude respectively as a false-color polar plot as obtained from the 9-element square array when excited using the clean-beam excitation as illustrated in Figure 5b. Conversely, Figure 6c and 6d shows the same case but without the effects of mutual coupling being taken into account. Here, the main effect is on the cross-polar pattern but it is crucial to have this information so that the overall cross-polar performance of the CATR can be accurately computed in the QZ.

IV. Optimisation Of Quiet Zone Size Using The Array Feed

In this section, we apply a simple genetic optimiser to change the array element excitation to give a feed pattern that would offer near uniform illumination across the main part of the CATR reflector thereby minimising the amplitude taper within the CATR QZ, corresponding to a necessary first step in developing more sophisticated reflector illuminations. A simple target feed pattern of requiring constant amplitude illumination across ±7° degrees, which represents the centre 1m of the CATR reflector's projected cross-sectional aperture in the AUT test-zone was used in this initial study. In addition, a symmetrical pattern was specified so that the amplitude and phase excitation of just the array element numbers 1 to 4 was optimised, the remaining elements being excited based on symmetry. Table I presents the resulting amplitude and phase excitations that were bred using this optimisation technique.

TABLE I. Array Element Excitations.

Element Number	***1***	***2***	***3***	***4***	***5***	***6***	***7***	***8***	***9***
Amplitude	1.0000	0.6737	0.4489	0.7282	0.4489	0.6737	0.4489	0.7282	0.4489
Phase	29.91°	55.39°	120.21°	32.37°	120.21°	55.39°	120.21°	32.37°	120.21°
Quantized Phase	0.0°	0.0°	180.0°	0.0°	180.0°	0.0°	180.0°	0.0°	180.0°

These results were achieved using a simple optimisation process using a root of the sum of the squares (RSS) penalty function and took a little over 3,000 iterations to converge to the results shown. However, using the array analysis described above means that on a high-end PC, each iteration took just under 1 second to complete compared to a full one pass CEM simulation of the array (for example using Feko) taking in excess of 30 minutes, corresponding to a speed up in the order of a factor of 1800 times.

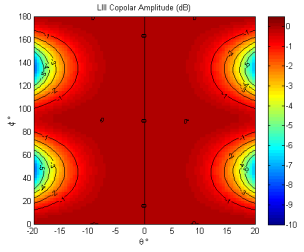

Figure 7a. Copolar polar spherical plot of far-field amplitude.

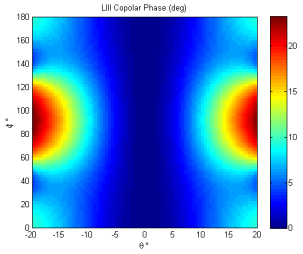

Figure 7b. Copolar polar spherical plot of far-field phase.

Figure 7 shows false colour amplitude and phase plots of the radiation cuts for the azimuthal angle ϕ ranging from 0° to 180° over the polar angle θ range of ±20°. The reduced polar angular range corresponded to the maximum pattern angle of ±14° subtended by the CATR reflector at the feed when the feed is optimally aligned. From inspection of Figure 7, the uniformity over the ±7° region is very evident. Figure 8 shows the optimised amplitude feed pattern for both co-polar and cross-polar fields plotted on a normal polar grid (*i.e.* true-view [1]). To achieve a practical array phase quantisation will be required and Figure 9 shows the radiation patterns of the feed using just the 0° and 180° degree phase values for the elements shown in the bottom row of Table I. In general it is more difficult to implement arbitrary phase changes across a wide-bandwidth and as such the ability to use phases of only 0° and 180° (where the waveguide feed is simply rotated by 180° in the transverse plane) becomes highly desirable.

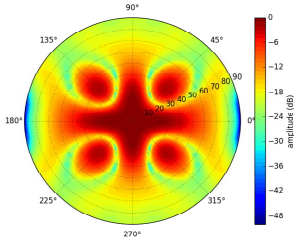

Figure 8a. Polar plots of the co-polar pattern of the optimised array feed shown in Fig. 7 using excitation shown in Table I.

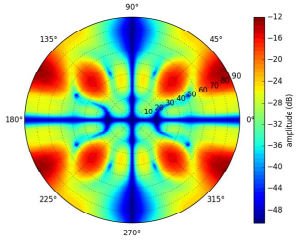

Figure 8b. Polar plots of the cross-polar pattern of the optimised array feed shown in Fig. 7 using excitation shown in Table I.

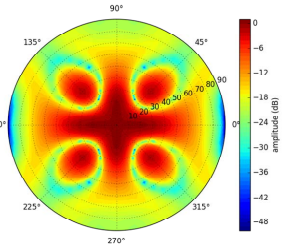

Figure 9a. As Figure 8a but using the quantised phase values shown in the bottom row of Table I.

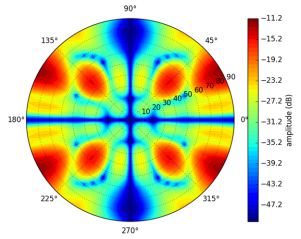

Figure 9b. As Figure 8b but using the quantised phase values shown in the bottom row of Table I.

Very little difference is seen and Figure 10 compares the 0°,45° and 90° radiation pattern amplitude cuts with and without this phase quantisation, the quantised phase amplitude pattern raising very slightly to the edge of the reflector at ±14°. The effects of using mutual coupling in the calculation of the array radiation pattern is shown in Figure 11 and is predominantly seen in the cross-polar pattern, shown, where a peak increase by about 2.5dB when mutual coupling is included. However, this is at a polar angle of 40° which is well outside the reflector illumination range.

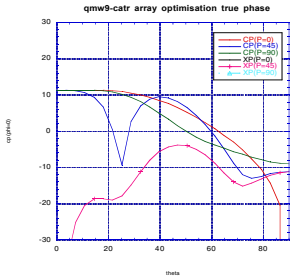

Figure 10a. Comparison of 0°, 45° and 90° pattern cuts using array excitation with the full phase.

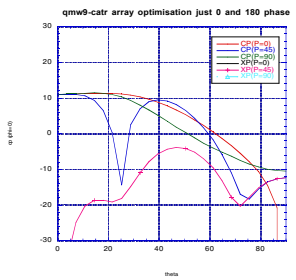

Figure 10b. Comparison of 0°, 45° and 90° pattern cuts using array excitation with the quantized phase.

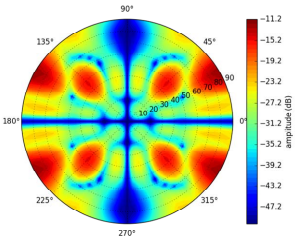

Figure 11a. Quantised array cross-polar amplitude pattern with mutual coupling included in the simulation

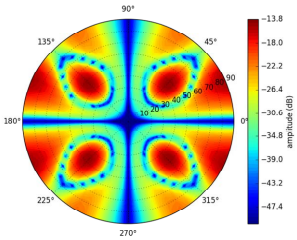

Figure 11b. Quantised array cross-polar amplitude pattern without mutual coupling included in the simulation

V. CATR Performance With Optimised Array Feed

In this section we take the optimised array feed pattern from the previous section and use it to compute the CATR QZ. Figure 12 shows the modelled fields illuminating the CATR reflector when using the optimised array as a feed. Here, the strong illumination on the left hand edge of the reflector is a result of the reduced spherical free-space loss factor, and can be compensated by having a tapered target pattern for the array in future optimisations. The increased uniformity of the pattern over the corrugated horn is evident by comparing this with the pattern shown in Figure 3 where consistent scales are used.

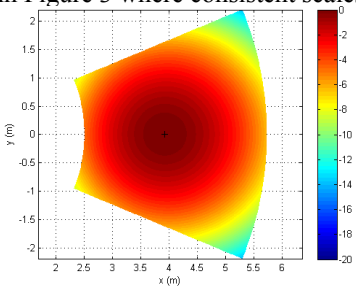

Figure 12. Simulated CATR field using the optimised 9-element array and exact phase values shown in the table of figure 7, *cf.* Figure 3.

The resulting predicted QZ amplitude in the *x* and *y* axis principal cuts is shown in Figure 13 indicating very low field taper over the nominal 1m QZ formed from the centre of the CATR reflector. The best fit 2nd order polynomial that is used to determine the QZ taper is shown in red plotted across the specified QZ span, which in this case was 1m.

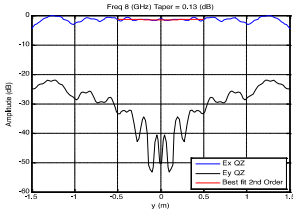

Figure 13a. Principal plane cuts of CATR QZ using the optimised array feed of Fig. 8 y-axis cut. Field taper in y-axis = 0.13dB.

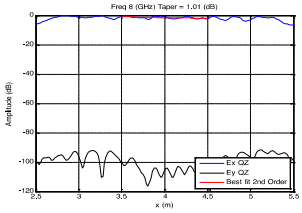

Figure 13b. Principal plane cuts of CATR QZ using the optimised array feed of Fig. 8 x-axis cut. Field taper in x-axis=1.01dB.

Figure 14 summarises QZ results for untreated reflector edge using both corrugated horn and array feed comparing amplitude taper and ripple (14a), phase ripple (14b). Clearly these results indicate that, due to reflector edge diffraction, the QZ ripple is too high for this CATR facility to operate at 8GHz with either the corrugated horn or array feed. However, we now use our prediction software to demonstrate how the use of reflector edge serrations can drastically improve the CATR QZ performance.

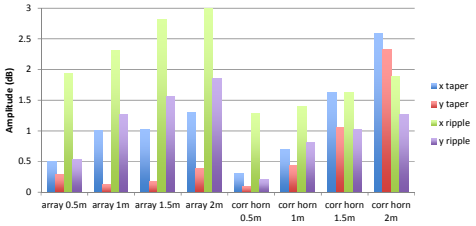

Figure 14a. Summary of results for untreated reflector edge with both corrugated horn and array feed comparing amplitude taper and ripple.

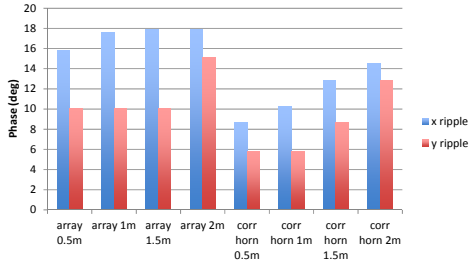

Figure 14b Summary of results for untreated reflector edge with both corrugated horn and array feed comparing phase ripple.

In Figure 15 we show two types of serrations applied to the reflector edge, a shallow serration, typically 7λ in depth, and a deeper serration, ranging from 7λ to 17λ along the reflector straight sides where diffraction is likely to be strongly cumulative in the QZ.

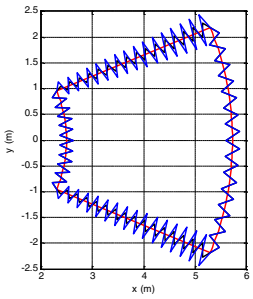

Figure 15. Two designs of serrated edge used to control the QZ performance. Red is un-serrated; Black is shallow triangular serrations, 7l high serrations on all sides; Blue is deeper triangular serrations, 7l high serrations on curved sides, up to 17l high serrations on straight sides.

In the case of shallow serrations Figure 16 shows summary results for the QZ amplitude taper and ripple and QZ phase ripple, the scaling is identical to that for the untreated reflector results of Figure 14 and so can be directly compared. Clearly, significant improvement in both phase and amplitude ripple is seen, and if we take as a usability criteria of a maximum amplitude taper and ripple of 1dB and maximum phase ripple of 10° then both the array feed and corrugated horn can achieve QZ sizes approaching 1.5m. It is worth noting the reduced amplitude taper offered by the array feed was the intended design goal for this study. Conversely, Figure 17 shows similar summary results for the case of the deep serration design where even stronger reduction in amplitude and phase ripple is seen, confirming the view that the straight edge of the reflector is a significant contributor to diffraction reaching the QZ.

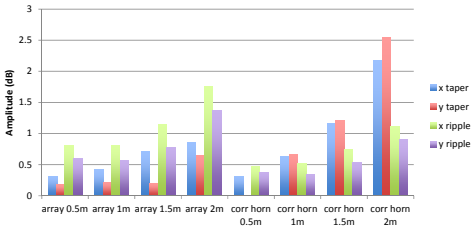

Figure 16a. Summary of results for shallow serrations on the reflector edge with both corrugated horn and array feed comparing amplitude taper and ripple.

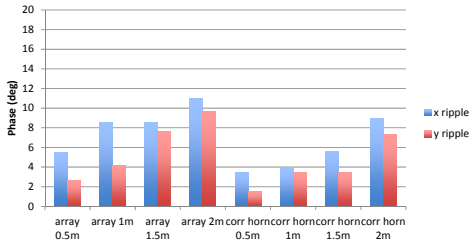

Figure 16b. Summary of results for shallow serrations on the reflector edge with both corrugated horn and array feed comparing phase ripple.

From these results it is clear that the QZ for the array is now close to 2m whereas that for the corrugated horn remains around 1.5m due to the far higher amplitude taper confirming the improvement in the efficiency with which the CATR reflector is used.

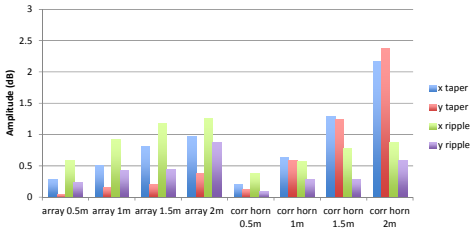

Figure 17a. Summary of results for deep serrations on the reflector edge with both corrugated horn and array feed comparing amplitude taper and ripple.

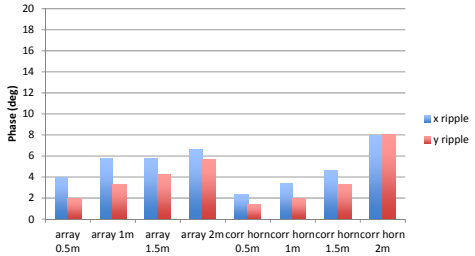

Figure 17b. Summary of results for deep serrations on the reflector edge with both corrugated horn and array feed comparing phase ripple.

VI. Summary And Conclusions

In this paper we have presented preliminary results of an ongoing study to investigate the use of an array feed with a single offset reflector CATR with the aim of improving and enlarging the QZ offered by a given reflector. Building on our previous work on efficient modelling of the CATR EM performance and coupling this with our previous work on mode based mutual coupling analysis of array antennas we have been able to demonstrate that we can optimise the CATR array feed to reach a desired QZ performance criteria in a highly efficient manner. At this stage of our research we have employed a simple optimisation process and used a very simple optimisation criteria which comprised requiring a flat amplitude and phase function over the centre 1m QZ. Using this feed with a plane edged reflector our analysis has confirmed the general view that to achieve acceptable QZ performance serration treatment of the reflector edges are required. Using a serrated edge treatment in our model indeed shows the power of applying serrations, a commonly employed strategy used with many commercial CATRs, and combining this with an array feed has demonstrated that some improvement can be seen in usable QZ size. In addition we have shown that for our simple optimised array we could quantise the required array element excitation phase to just 0° and 180°, offering a very practical and wideband network implementation.

As this paper summarises ongoing research, our future aim is to achieve the QZ performance indicated by the deep serrated edge reflector reported here, but using no serrations and instead achieving low reflector edge fields by optimising the array feed pattern for low edge illumination. This will require a more sophisticated optimiser and will very probably require additional array elements. The potential power of such an approach is that we can optimise the feed excitation for each operating frequency maximising the QZ volume for a given CATR facility without increasing the size of reflector or test chamber.

References

[1] C.G. Parini, S.F. Gregson, J. McCormick, D. Janse van Rensburg "Theory and Practice of Modern Antenna Range Measurements", IET Press, 2014, ISBN 978-1-84919-560-7.

[2] M. Philippakis, C.G. Parini, "Compact Antenna Range Performance Evaluation Using Simulated Pattern Measurements", IEE Proc. Microw. Antennas Propag., Vol. 143, No. 3, June 1996, pp. 200-206.

[3] C.G. Parini, R. Dubrovka, S.F. Gregson, "CATR Quiet Zone Modelling and the Prediction of 'Measured' Radiation Pattern Errors: Comparison using a Variety of Electromagnetic Simulation Methods" AMTA October 2015.

[4] C.G. Parini, R. Dubrovka, S.F. Gregson, "Computational Electromagnetic Modelling of Compact Antenna Test Range Quiet Zone Probing: A Comparison of Simulation Techniques", EuCAP, Davos, 2016.G.L. James, "Geometrical Theory of Diffraction for Electromagnetic Waves", 3rd Edition, IET Press, 2007.

[5] D.J. Wayne, J. McKenna, S.T. McBride, "Advancements in Achieving What is Asked of a Compact Range", 35th Annual AMTA Symposium, Columbus, Ohio, October 2013.

[6] J.P. McKay, Y. Rahmat-Samii, "An Array Feed Approach to Compact Range Reflector Design", IEEE Trans. AP vol. 41, pp 448-457, April 1993.

[7] D. Kitchener, K. Raghavan, C.G. Parini, "Mutual Coupling in a Finite Planar Array of Rectangular Apertures", Electronic Letters, Vol. 23, No. 11, pp. 1169-1170, 1987

[8] T.S. Bird, "Improved solution for mode coupling in different-sized circular apertures and its application", IEE Proc. H. Microwaves, Antennas Propag., Vol. 143, pp. 457-464, 1996.

[9] A.D. Olver, C.G. Parini, "Millimetre-wave Compact Antenna Test Range", JINA Nice, November 1992.

[10] C. G. Parini; D. Kitchener, "The Importance of Mutual Coupling in the Analysis of Finite Arrays of Rectangular Apertures", 19th European Microwave Conference, 1989, Pages: 265 - 271, DOI: 10.1109/EUMA.1989.333976 .

[11] N.A. Adatia, A.W. Rudge, C.G. Parini, "Mathematical modelling of the radiation fields from microwave primary feed antennas", IEE International conference on Antennas & Propagation, London, November 1978.

[12] R.F. Dubrovka, "Analysis of finite antenna arrays from the open ends of axisymmetric longitudinally-irregular structures", Izvestiya VUZ: Radioelektronika, Vol. 39, No. 10, pp. 50-63, 1996, 1996.